BIOCHEMISTRY
including biophysical chemistry & molecular biology

Article

pubs.acs.org/biochemistry

Primary and Secondary Dimer Interfaces of the Fibroblast Growth Factor Receptor 3 Transmembrane Domain: Characterization via Multiscale Molecular Dynamics Simulations

Tyler Reddy,[†] Santiago Manrique,[†,‡] Amanda Buyan,[†] Benjamin A. Hall,[†,§] Alan Chetwynd,[†] and Mark S. P. Sansom*[,†]

[†]Department of Biochemistry, University of Oxford, South Parks Road, Oxford OX1 3QU, U.K.

[‡]Division of Structural Biology, Wellcome Trust Centre for Human Genetics, University of Oxford, Oxford OX3 7BN, U.K.

Supporting Information

ABSTRACT: Receptor tyrosine kinases are single-pass membrane proteins that form dimers within the membrane. The interactions of their transmembrane domains (TMDs) play a key role in dimerization and signaling. Fibroblast growth factor receptor 3 (FGFR3) is of interest as a G380R mutation in its TMD is the underlying cause of ∼99% of the cases of achondroplasia, the most common form of human dwarfism. The structural consequences of this mutation remain uncertain: the mutation shifts the position of the TMD relative to the lipid bilayer but does not alter the association free energy. We have combined coarse-grained and all-atom molecular dynamics simulations to study the dimerization of wild-type, heterodimer, and mutant FGFR3 TMDs. The simulations reveal that the helices pack together in the dimer to form a flexible interface. The primary packing mode is mediated by a Gx_3G motif. There is also a secondary dimer interface that is more highly populated in heterodimer and mutant configurations that may feature in the molecular mechanism of pathology. Both coarse-grained and atomistic simulations reveal a significant shift of the G380R mutant dimer TMD relative to the bilayer to allow interactions of the arginine side chain with lipid headgroup phosphates.

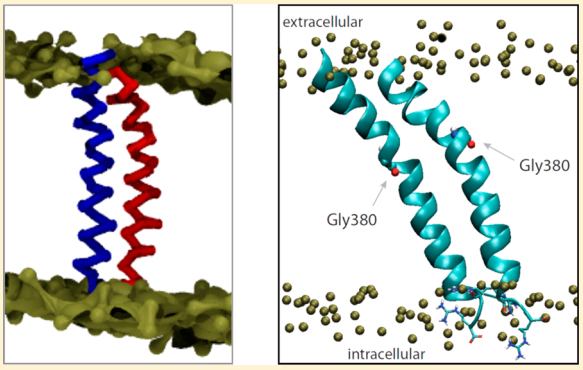

Receptor tyrosine kinases (RTKs) are single-pass membrane proteins. They have an extracellular ligand-binding ectodomain, an α-helical single-transmembrane domain (TMD), and an intracellular kinase domain.[1] They form dimers within the membrane, and a number of nuclear magnetic resonance (NMR) structures of TMD dimers in membrane-like environments have been determined.[2−8] However, in the absence of a high-resolution structure for an intact RTK, important aspects of the conformational dynamics of the TMD dimers in relation to signaling remain unknown.

Many RTKs are important in the context of human disease. Fibroblast growth factor receptor 3 (FGFR3) is of particular interest as a G380R mutation in its TMD is the underlying cause of ∼99% of the cases of achondroplasia, the most common form of human dwarfism.[9] Although the genetic basis for achondroplasia has been known for nearly two decades, the molecular mechanism of pathology remains uncertain. FGFR3 is a negative regulator of bone growth, and there is experimental evidence of an increased level of signaling by the mutant receptor.[10] It is thus of interest to understand the effects of the G380R mutation on the behavior of the TMD dimer at a fundamental biophysical level.

The free energies of dimerization, as measured by Förster resonance energy transfer in a 1-palmitoyl-2-oleoyl-*sn*-glycero-3-phosphocholine (POPC) lipid bilayer for wild-type and G380R TMD peptides, match one another within the bounds of experimental uncertainty,[11] indicating that perturbation of dimerization propensity per se is unlikely to be the key effect of this particular mutation. Significantly, neutron diffraction and oriented circular dichroism indicate a 5 Å "vertical" shift of the G380R mutant peptide relative to the center of a lipid bilayer.[12] Thus, there is an apparent conceptual disconnect between the significant shift in position relative to the lipid bilayer and the unperturbed association free energy of the mutant FGFR3 TMD, which merits further investigation. Importantly, recent experimental evidence indicates that a different pathogenic mutation of FGFR3, A391E, leads to an increase in dimer stability (−1.5 kcal/mol) in a manner independent of whether the FGFR3 TMDs are studied in isolation or with their large ectodomains attached.[13] This supports the validity of studying the interactions of FGFR3 TMDs in isolation to improve our

Received: November 26, 2013
Revised: January 2, 2014
Published: January 3, 2014

understanding of the conformational dynamics of the more complex intact receptor. It also indicates that some mutations may act by changing dimer stability while other mutations may perturb TMD dimers in a different fashion.

There have been a number of NMR studies of TMD dimers from a range of RTKs, including the ErbB receptors[2−5] and the EphA receptors.[6,7] These have revealed a variety of packing modes and motifs. Furthermore, a combination of experimental[14,15] and computational[1,16] approaches have recently emphasized the importance of the multiple modes of interaction of TMDs within dimers that play a key role in signaling by RTKs.[17] A recent NMR structure of the FRFR3 TMD dimer[8] in a detergent [DPC/sodium dodecyl sulfate (SDS)] micelle environment, which reveals a helix packing mode dominated by an extended hydrophobic heptad, has been interpreted in the context of mapping of the location of pathogenic mutations as suggesting a putative alternative helix interface that is formed upon receptor activation.

Molecular dynamics (MD) and related simulations can provide insights into TMD dimerization, both of model systems such as glycophorin (GpA, e.g., refs 18−21) and of RTKs, especially ErbBs (e.g., refs 14, 16, 22, and 23). To date, relatively short time scale (50 ns) atomistic simulations have been performed on FGFR3 TMDs, with selection of starting configurations from a Monte Carlo search in a simplified implicit bilayer model,[24] suggesting multiple packing modes for the TMD helices within the dimer.

Here we study the dimerization of FGFR3 TMD constructs over extended (microsecond) time scales using coarse-grained (CG) MD simulations.[25] This approach has been previously used to successfully model GpA[26] TMD dimerization, providing results consistent with high-resolution experimental structures and mutagenesis results. Representative TMD dimers formed in these CG simulations are refined by atomistic (AT) MD simulations, providing a multiscale approach to FGFR3 TMDs, as used in, e.g., previous studies of integrin TMD dimers.[27] We focus on the G380R mutation and compare FGFR3 wild-type, heterodimer, and mutant homodimer TMDs in terms of both helix−helix and protein−lipid interactions. Significantly, our simulations of the wild-type TMD reveal a predominant packing mode that corresponds to the activated state proposed by Bocharov et al.[8]

MATERIALS AND METHODS

CG Simulations. Coarse-grained simulations (Table 1) were performed in GROMACS version 4.0.x[28] using a previously described[25] local version of the MARTINI force field,[29−31] which employs an approximate 4:1 mapping of heavy atoms to representative particles. The CG simulations were conducted at 323 K with separate temperature coupling for protein, lipid, and solvent using the Berendsen thermostat.[32] Time steps of 40 fs were used with frames written every 400 ps. Coulomb and van der Waals interactions were shifted to 0 between 0 and 12 Å and between 9 and 12 Å, respectively. Semi-isotropic pressure coupling was performed using the Berendsen algorithm with a 1.0 ps time constant, a 5×10^{-6} bar^{-1} compressibility, and a 1.0 bar reference pressure. Replicate simulations employed different starting velocity seeds. Final simulation box sizes varied slightly, with approximate dimensions of 10.5 nm × 10.5 nm × 11.5 nm. WT, WT/G380R heterodimer, and G380R homodimer systems had slightly different compositions with approximately 330 POPC molecules, 6400 water molecules, and a small number of neutralizing Cl^- ions.

Table 1. Summary of Simulations

TMD	force field	duration
FGFR3		
WT	CG, modified MARTINI[a]	10 × 5 μs[c] and 20 × 1 μs[d]
WT/G380R	CG, modified MARTINI	10 × 5 μs[c]
G380R	CG, modified MARTINI	10 × 5 μs[c] and 20 × 1 μs[d]
WT	AT[b]	0.1 μs
G380R	AT	2 × 0.1 μs
GpA (control)		
WT	CG, modified MARTINI	5 × 5 μs

[a]The modified MARTINI force field is as described in ref 25. [b]Atomistic simulations were run using the GROMOS force field[37] gromos43a1. [c]These simulations are the basis of the main analysis shown in Figures 1−4. The sequence used was as previously employed in ref 10 with the G380 residue in bold (RRAGSVYAGIL-SYG[380]VGFFLFILVVAAVTLCRLR). [d]These simulations were used to generate representative structures from which to initiate the atomistic simulations. The sequence DEAGSVYAGIL-SYG[380]VGFFLFILVVAAVTLCRLR was employed.

The TMDs were modeled as ideal α-helices. The initial separation between the TMD helices in the CG simulations was ∼55 Å (see Figure 1A), the same value used in previous GpA CG simulations,[26] and outside the 12 Å long-range interaction cutoff for this force field. The initial systems with separated helices were generated by 200 ns simulations, in which POPC bilayers were self-assembled around position-restrained protein TMDs, as described previously.[33]

Atomistic Simulations. Initial AT simulation systems were generated from representative CG TMD dimer structures using our CG2AT protocol as described previously.[34] Representative average structures were obtained using the g_cluster module of GROMACS. The resulting AT system was energy minimized and equilibrated (duration of 1 ns) with a position restraint on protein Cα atoms (force constant of 10 kJ mol^{-1} $Å^{-1}$). Unrestrained simulations were performed with a time step of 2 fs and a total duration of 100 ns per simulation. A semi-isotropic pressure of 1 bar was applied using a Parinello-Rahman barostat,[35] and the temperature was maintained at 323 K with a Berendsen thermostat.[32] Electrostatic interactions were modeled using a particle mesh Ewald summation (cutoff distance of 10 Å, also used for van der Waals interactions). The bond lengths were restricted using the LINCS algorithm.[36] GROMACS version 4.5.4[28] was used in combination with the GROMOS96 43a force field.[37]

Trajectory Analysis and Visualization. CG-MD trajectories were exposed using the MDAnalysis library[38] and parsed using in-house Python code detailed in the algorithm descriptions provided in the Supporting Information. AT-MD trajectories were analyzed using GROMACS version 4.5.4[27] tools. Visualization was performed with VMD.[39]

RESULTS AND DISCUSSION

TMD Dimerization. We performed ensembles of 5 μs duration dimerization simulations for wild-type (WT) and mutant (see Table 1) FGFR3 TMD helices and for (control) GpA TMDs, with the two TMD monomers initially separated by ∼55 Å in POPC bilayers (Figure 1). As previously seen for GpA,[26] there was stochastic variation in the time required for initial dimer formation (Figure S1 of the Supporting

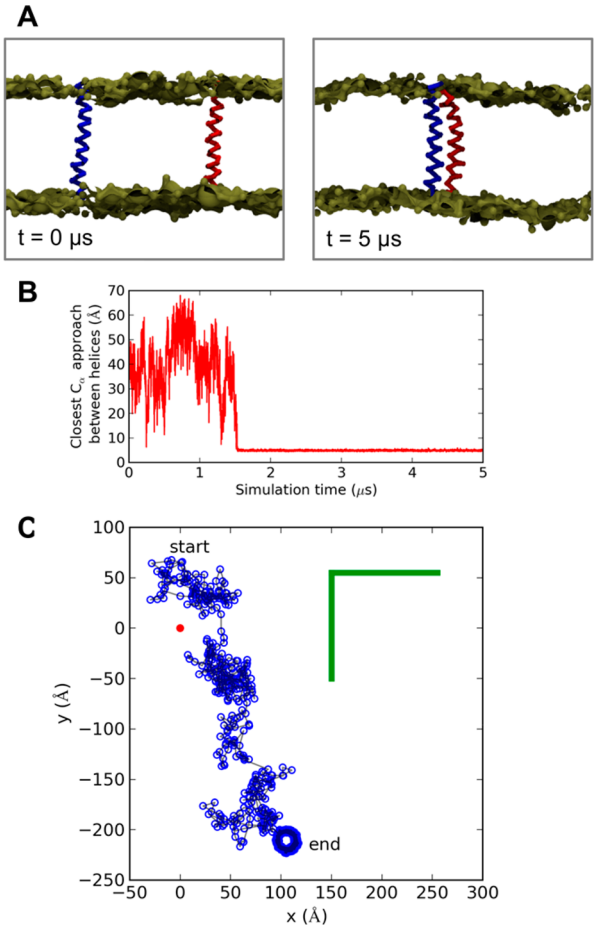

Figure 1. (A) Initial (t = 0 μs) and final (t = 5 μs) configurations of a WT FGFR3 CG simulation showing the two helices as C_α traces in red and blue with the bronze spheres corresponding to a surface representation of the phosphate particles of the lipids. Other lipid and solvent particles have been omitted for the sake of clarity. (B) C_α helix–helix approach shown as a function of time for the same WT FGFR3 CG simulation as in panel A. (C) Relative motion of the centroid of helix 2 (blue) in the reference frame of the centroid of helix 1 (red) shown for the same FGFR3 WT CG simulation as in panels A and B. Coordinates of helix 2 are plotted every 10th frame of the simulation (i.e., every 4 ns) in the x–y plane (which is approximately equivalent to the bilayer plane). The approximate size of the simulation box in the x–y plane is shown in green.

Information), corresponding to the use of random initial velocities (consistent with a Maxwellian distribution at the stated temperature) for each simulation within an ensemble. There did not seem to be any substantial difference in the time to dimer formation among the FGFR3 WT, WT/G380R, and G380R simulations, although much larger ensembles (typically of ≥100 simulations) would be needed to more accurately explore any differences in dimerization times. In many simulations, one helix wanders substantially within the bilayer plane before dimer formation relative to the other helix (Figure 1C). Thus, the stochastic dimerization times and substantial translational (and rotational) motions of the helices relative to one another within the bilayer plane are consistent with a simulation protocol that is not biased toward formation of a particular dimer interface. Both the GpA and the FGFR3 TMDs formed stable dimers in our CG simulations, with no observations of subsequent dissociation of the helices. Indeed, atomistic[14] simulations of the related EGFR TMDs indicate that extended (>10 μs) simulations are likely to be needed to observe TMD dimer dissociation events. We examined the bilayer thickness around the TMDs (Figure S2 of the Supporting Information), and although a small degree of thinning (1–2 Å) was observed adjacent to the FGFR3 TMDs, this was the same before and after dimerization, suggesting that the bilayer thickness is unlikely to have a major effect on dimerization.

Having confirmed the formation of stable dimers in an unbiased fashion in our simulations, we have analyzed the properties of the dimer configurations in detail. Our control GpA TMD dimers in POPC bilayers consistently exhibited right-handed helix crossing angles (Figure 2A), as previously reported for GpA simulations in DPPC,[19,20,26] and consistent with experimental NMR structures of the GpA TMD.[40,41] In contrast, the FGFR3 TMD helices did not show a strong preference for left- or right-handed helix packing, instead exhibiting bimodal distributions of crossing angles. There is a

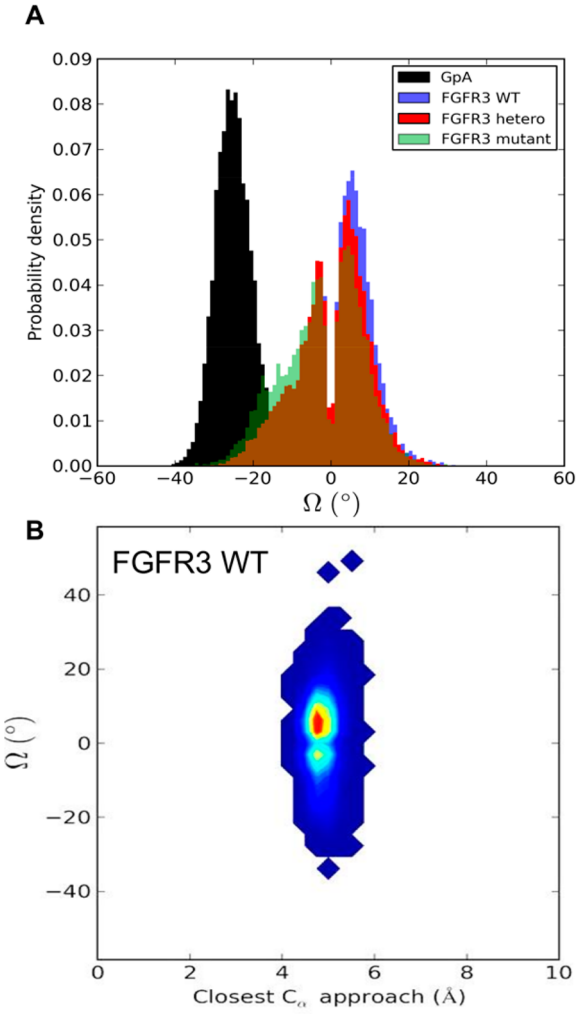

Figure 2. (A) Helix crossing angle (Ω) distributions for the merged (see Table 1) FGFR3 WT (blue), FGFR3 WT/G380R heterodimer (red), FGFR3 G380R homodimer (green), and GpA (control, black) simulations. Every 25th frame (i.e., every 10 ns) of the constituent trajectories was parsed and included in the histograms only if the helices were dimerized (10 Å interhelix centroid distance cutoff). (B) Helix crossing angle (Ω) vs C_α helix–helix approach distribution for the FGFR3 WT simulations, using an ascending blue to yellow to red heat map.

dx.doi.org/10.1021/bi401576k | *Biochemistry* 2014, 53, 323–332

slight preference for left-handed helix packing for wild-type FGFR3 relative to that of the WT/G380R heterodimer and G380R mutant homodimers. The bimodal distribution may result from FGFR3 helices adopting different crossing angles as they oscillate closer or farther apart in the dimer, although the helix crossing angles appear to be largely independent of the closest approach distance of the helices (Figure 2B), with a bimodal distribution at a single optimal distance. The FGFR3 helices thus form stable dimers but exhibit a broad range of helix crossing angles suggestive of a "looser" interface than in, for example, GpA. To probe their relative motions in the bilayer, the correlation coefficients for the z coordinates of the geometric centers of each helix were calculated before and after dimer formation (Figure S3 of the Supporting Information). As expected, helix displacement motions were not correlated before dimer formation but were strongly correlated after a dimer was formed. Significantly, GpA exhibits a more strongly correlated dimer motion ($R \sim 0.8$) than all of the FGFR3 TMD dimers ($R \sim 0.6$). This is consistent with, for example, TOXCAT studies,[42] suggesting the GpA TMD dimer is more stable than the FGFR3 dimer. Given the somewhat weaker correlation of translation motion of FGFR3 helices within the dimer and the bimodal helix crossing angle distribution, we decided to examine the nature of the helix dimer interface more closely.

To identify the predominant residues within a (dynamic) interface, we calculated the normalized probability for each C_α residue on either helix to be in the top five closest interhelix contacts over the whole ensemble of simulations. To test this approach, the analysis was first performed on the GpA simulations. G79, G83, and T87 were identified as predominant contacts (Figure S4 of the Supporting Information). Because these three residues have previously been identified as experimentally crucial interfacial contacts (see, e.g., ref 43), this analytical approach may confidently be applied to predict interfacial residues in the FGFR3 TMD.

Residues G370, A374, S378, and G382 (which form three consecutive small-x_3-small motifs) and also R397 stand out as important contacts from FGFR3 wild-type, heterodimer, and mutant homodimer simulations (Figures 3 and 4A), and other candidates are spaced at three- or four-residue intervals, consistent with the identification of a helical interface. It is noteworthy that residues 380 and 391, involved in achondroplasia and Crouzon syndrome, respectively,[44] do not feature prominently in the closest contacts in FGFR3 dimer configurations. This is consistent with the lack of an effect of the G380R mutation on dimerization propensity.[11] G370, which is prominent in the closest contacts, is mutated to Cys in type 1 thanatophoric dysplasia, which is much more severe than achondroplasia and normally neonatal lethal.[45] Thus, phenotype severity may, at least in part, reflect the proximity of the point mutation to the dimer interface. Furthermore, G370 was recently identified at the dimer interface by site specific infrared dichroism,[46] and the propensity for disulfide formation in FGFR3 decreases in the following order: C370 > C371 > C375.[47] Interestingly, R397, which is one of the top three major FGFR3 contacts we identify, is part of the CRLR C-terminal tetrapeptide that, if removed, increases the dimerization propensity of FGFR3 to match that of GpA.[46]

Alternative Dimer Interfaces. The biological and experimental correlations with our candidate FGFR3 dimer interface residues are encouraging. However, the identification of a small set of major dimer contact residues does not explain

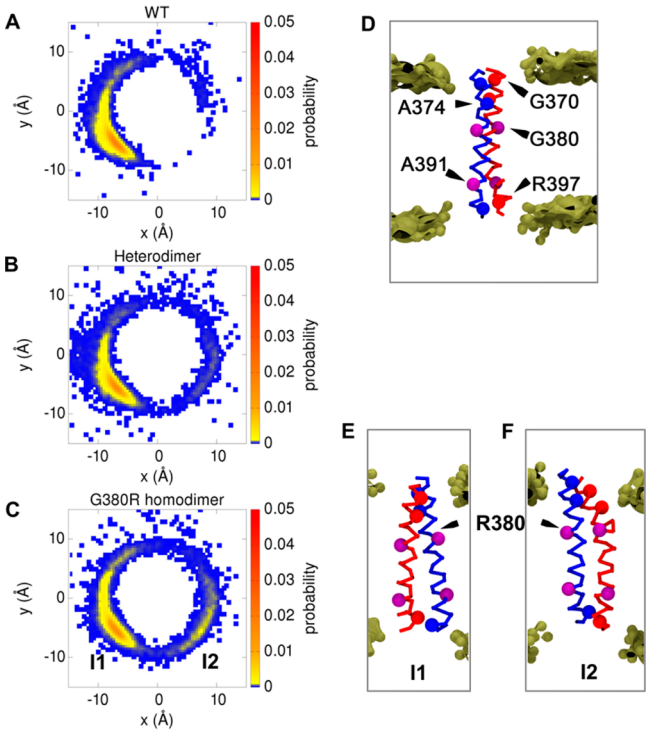

Figure 3. (A–C) Positional probability of the geometric center of helix 2 relative to helix 1 in the x–y plane shown as a nonlinear (ascending from blue to yellow to red) heat map for the FGFR3 WT (A), FGFR3 WT/G380R heterodimer (B), and FGFR3 G380R homodimer (C) simulations. To generate these maps, each frame of a simulation is aligned by root-mean-square deviation fitting of helix 1 to the configuration of that helix in the first frame of the FGFR3 WT simulations. (D) Representative structure of the WT helix dimer, corresponding to the maximal probability in panel A. The C_α atoms of key residues forming the predominant interfacial contacts [G370, A374, and R397 (see the main text and Figure 4)] are shown as red and blue spheres, while the disease-related residues G/R380 and A391 are colored purple. The bilayer phosphate particles are shown as bronze spheres (surface representation). (E) Representative structures of the G380R mutant homodimer, corresponding to the two peaks in probability I1 (E) and I2 (F) in panel C.

how FGFR3 dimers can exhibit both left- and right-handed helix crossing angles. To explore the possibility of alternative dimer interfaces, one helix in each simulation was fixed to a reference structure and positional probability of the second helix in this reference frame determined (Figure 3). This analysis reveals a primary dimer interface for FGFR3 WT, heterodimer, and mutant TMDs. Importantly, a secondary dimer interface progressively begins to appear for the heterodimer and is most pronounced in the mutant homodimer simulations. Interestingly, tracking dimer configuration in this fashion as a function of simulation time revealed that there are discrete periods within a simulation when the dimer adopts one of the two interfaces along with a clear transition point from one interface to the other, rather than, e.g., a continuous switching between the two interfaces (Figure 5). There is, however, considerably more motion about the secondary interface, which is consistent with a lower-stability dimer configuration.

Further analysis of the motion of helix 2 relative to (fixed) helix 1 reveals a correlation of the polar angle (θ) defining the relative position of helix 2 within the bilayer plane with interhelix crossing angle [Ω (Figure S5 of the Supporting

dx.doi.org/10.1021/bi401576k | Biochemistry 2014, 53, 323–332

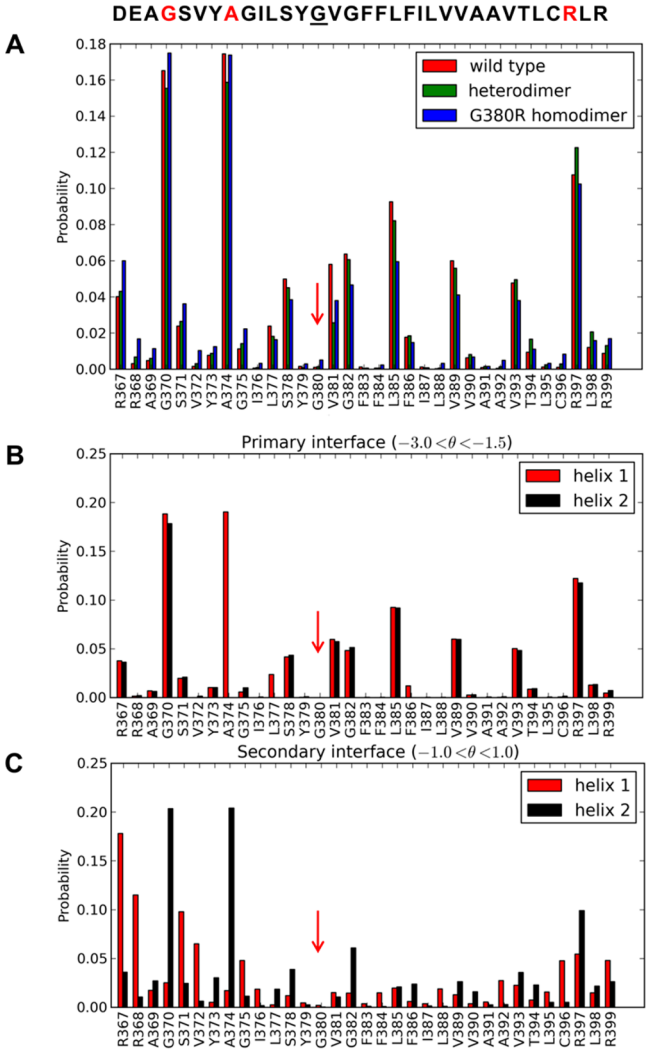

Figure 4. (A) Normalized frequency of occurrence for a residue to be in the five closest contacts between helices. A dimer is defined as a structure in which the interhelix (C_α particle) separation is <7 Å over all the CG simulations of an ensemble. Results are merged for both helices 1 and 2 of the WT (red), heterodimer (green), and G380R mutant homodimer (blue) simulations. (B) Normalized frequency of occurrence for a residue in the five closest contacts between helices [defined as a structure in which the interhelix (C_α particle) separation is <6 Å] for the primary (I1 in Figure 3) interface showing helices 1 and 2 in red and black, respectively. (C) Normalized frequency of occurrence for a residue in the five closest contacts between helices in the secondary (I2 in Figure 3) interface. The vertical red arrows indicate residue G380.

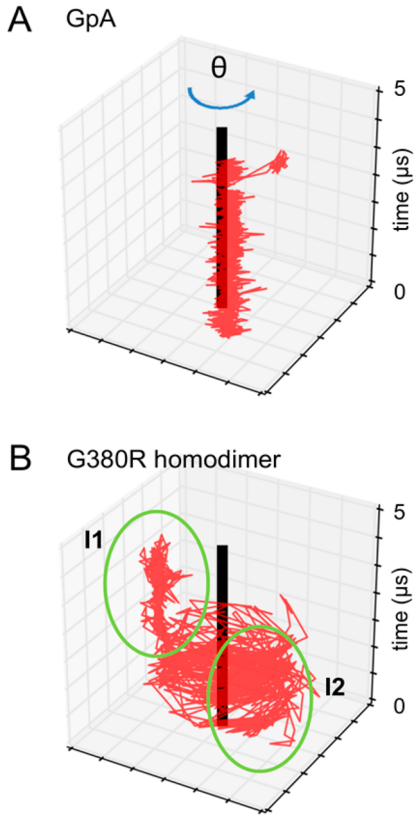

Figure 5. Position of the geometric center of helix 2 (red) relative to helix 1 (black) in the x−y plane as a function of time (vertical axis). This is shown for representative simulations from the (A) GpA and (B) FGFR3 G380R mutant homodimer ensembles. For the G380R simulation, the green rings indicate the primary (I1) and secondary (I2) interfaces (see Figure 3 and the text).

Information)]. Thus, the primary dimer interface (I1 in Figure 3) exhibits a bimodal helix crossing angle of ∼0°, while the secondary dimer interface (I2 in Figure 3) observed in the FGFR3 heterodimer and mutant homodimer exhibits a predominantly right-handed helix crossing angle. Using the value of θ as a means to classify dimer interfaces across all FGFR3 trajectories, we repeated the dimer interface contact analysis for the classified trajectories and discovered a striking loss of interfacial symmetry at G370, which is a prominent contact for both helices at the primary interface but for only one at the secondary interface (Figure 4B,C). The secondary dimer interface also loses symmetry at the important R397 contact.

The presence of a secondary dimer interface in FGFR3 mutant heterodimer and mutant homodimer configurations suggests that rearrangement of these TMDs may be a component of the molecular mechanism of pathology in achondroplasia. The rearrangement, a rotation of one helix relative to the other, may provide a gain of function to the attached intracellular kinase domains. Indeed, changes in helix packing within TMD dimers[48] have been suggested as possible activation mechanisms in, e.g., recent combined experimental and computational studies of EGFR[1,14] activation and on the basis of computational studies of FGFR3 dimers.[24] Furthermore, the oncogenic V664E TMD mutation in Neu (i.e., the rat homologue of ErbB2) prevents conformational switching between the active and inactive states.[49] Thus, the plasticity of the TMD helix dimer interfaces in RTKs seems likely to play a key role in conformational switching underlying receptor activation.

The G380R Mutation and Bilayer Interactions. Our results indicate that the G380R mutation promotes the adoption of a secondary interface, even though this residue is located opposite interfacial residues. Furthermore, experimental studies have indicated that the G380R mutation leads to a translation of the TMD along the bilayer normal.[12] To further explore the structural and functional implications of this mutation, we have examined the protein−lipid interactions and the positions of WT and mutant TMD dimers relative to the bilayer. Calculation of the average TMD dimer position relative to the bilayer normal (z position) suggests that in the CG

dx.doi.org/10.1021/bi401576k | Biochemistry 2014, 53, 323−332

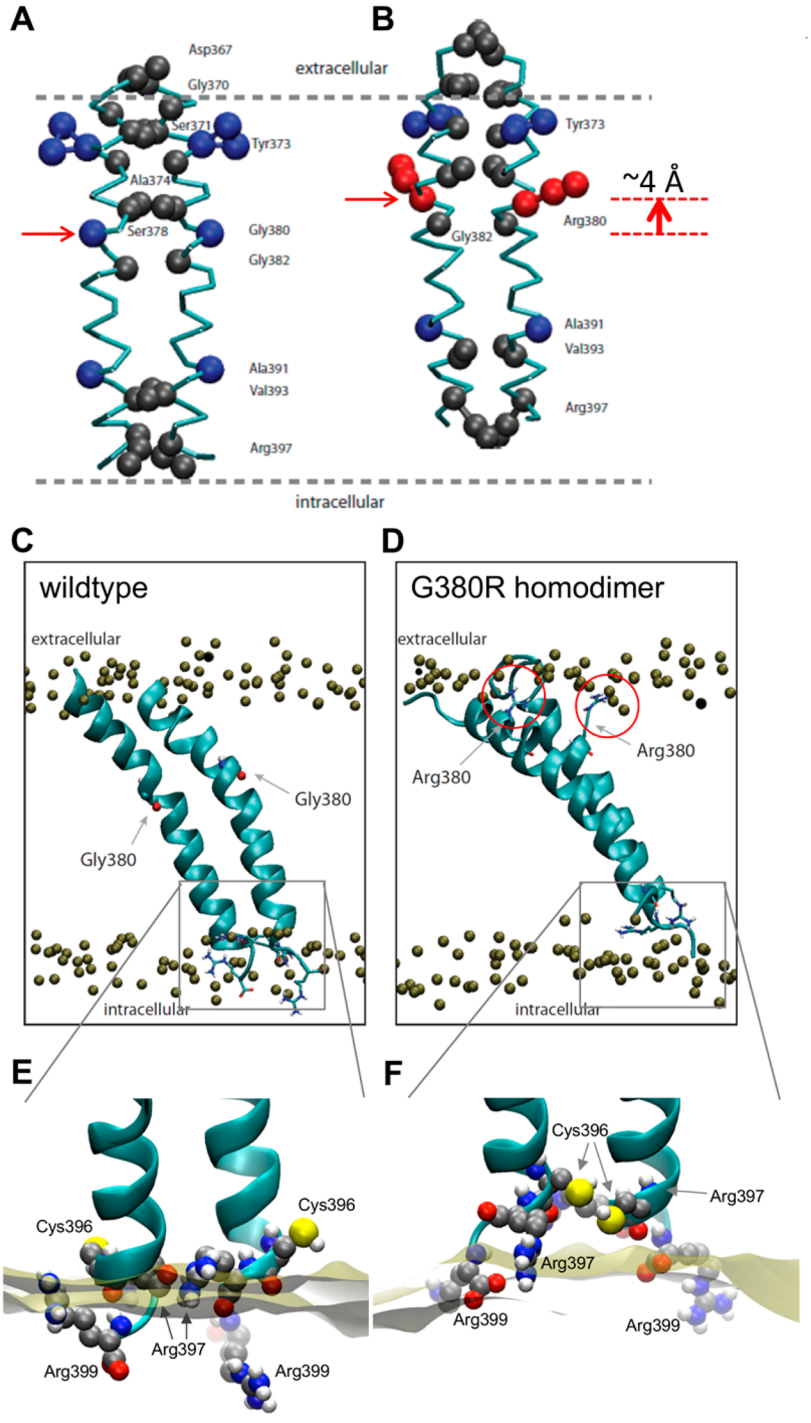

Figure 6. (A and B) Representative models corresponding to the primary helix–helix interface (I1 in Figure 3) for the wild-type (A) and G380R homodimer (B) CG simulations. The Cα backbone is colored cyan. The closest contact residues are shown as gray spheres and disease-related residues (Y373, G380, and A391) as blue spheres. The two dashed lines indicate the approximate position of the phosphate particles of the CG lipid bilayer. The horizontal arrows indicate the residue at position 380, G in the wild type and R (red) in the mutant. (C and D) Atomistic simulations of the wild-type (C) and G380R mutant (D) homodimer helix dimers starting from the structures shown in panels A and B, respectively. The final frames of the 100 ns AT-MD simulations are shown. The phosphorus atoms of the lipids are shown as bronze spheres. In panel C, the G380 atoms are shown; in panel D, the R380 side chains forming snorkelling interactions with lipid phosphates are shown in bond format and highlighted with red circles. (E and F) Detailed view of protein–lipid interactions at the inner membrane leaflet. The atoms of C396, R397, and R399 are shown as spheres, colored according to atom type. The bronze surface represents the position of the membrane phosphate particles. In the WT simulation (E), the $C_{396}RLR_{399}$ residues are located around the phosphate periphery whereas the G380R mutation (F) pulls those residues toward the membrane core, resulting in a rotation of the C-terminal TMD section.

simulation the G380R mutant induces a translation of ~4 Å along the bilayer normal toward the upper (i.e., extracellular) membrane leaflet. Clustering of structures from a second CG simulation ensemble with shorter durations but a higher repeat number (see Table 1) yielded representative structures for the primary interface (I1) TMDs of WT and G380R FGFR3

dx.doi.org/10.1021/bi401576k | *Biochemistry* 2014, 53, 323–332

(Figure 6A,B). The representative structure for the FGFR3 G380R dimer (Figure 6B) shows that both of the R380 side chains are directed toward the upper membrane leaflet where they are able to interact with the negatively charged phosphates of the lipid headgroups. These representative CG structures were converted to the corresponding atomistic models[34] to run short (0.1 μs) atomistic simulations (see Table 1). The final frame of the atomistic WT simulation represents a stable dimer, fully integrated into the lipid bilayer (Figure 6C). The primary dimer interface (I1) observed in the CG simulations is maintained. The final snapshot of the G380R mutant homodimer clearly shows the vertical translation of both Arg380 residues (Figure 6D), such that these side chains interact with the phosphate headgroups of the upper leaflet. This "snorkelling" effect of basic amino acid side chains in the hydrophobic membrane environment has been widely discussed in terms of stabilizing the localization of the TMD within bilayers (see, e.g., ref 50) and also has been suggested to regulate signaling across the membrane by integrins.[51] Comparing the movements of WT and G380R dimers relative to the membrane normal reveals an approximate difference in the z position of ~5.5 Å (Figure S6 of the Supporting Information), i.e., just a little more than in the CG simulations, and consistent with the different resolutions of the two methods. This agrees well with the displacement of the TMD in the mutant by 5 Å revealed by neutron diffraction studies.[12] The TMD helices also tilt relative to the bilayer in the AT-MD simulations, such that the helix tilt angle for the WT simulation reached an average of ~33° whereas the tilt of the corresponding G380R simulation reached an average of ~42°. However, more extended AT simulations may be needed to obtain reliable estimates of tilt angle distributions.[52]

In the WT TMD dimer, both of the R397 residues are located close to the lipid headgroup phosphates of the lower (inner) leaflet (Figure 6E). This allows the two R397 residues of adjacent helices to remain close to one another. This interaction is in agreement with our CG simulations, suggesting that R397 plays an important role in (lipid-mediated) TMD dimer formation (Figure 4A). Furthermore, our AT simulations confirm that both R399 residues reside in the cytoplasm and that both C396 residues are not involved in the dimer interface (Figure 6E).

Interestingly, concomitantly with the 5.5 Å translation induced by the G380R mutant, the C-terminal residues (i.e., $C_{396}RLR_{399}$) are pulled toward the core of the bilayer (Figure 6F). Consequently, the R399 side chains occupy energetically favorable positions at the membrane–water interface that are occupied by the R397 residues in the WT TMD dimer. Intriguingly, the R397 residues are moved closer toward the membrane center (resulting in some degree of local thinning of the bilayer), which forces them to adopt a more snorkelling conformation to retain the interaction of the guanidinium group with the lipid phosphates. This destabilizes the intermolecular R397–R397 interaction, resulting in more asymmetric rearrangement of the C-terminal region in which the C396 residues now form the main TMD dimer interaction. These findings support the suggestion derived from experimental data that conformational changes at the CRLR tetrapeptide may serve as a conformational switch between different states of activation and inactivation of the kinase.[46]

CONCLUSIONS

Overall, our results reveal the presence of multiple possible FGFR3 TMD dimer interfaces, with their relative propensities influenced by the presence of point mutations. In the case of the G380R mutation, interactions of the arginine side chain with lipid bilayer phosphates may play a role in shifting propensities. Interestingly, our observation of an asymmetric secondary interface was also reported for the G380R FGFR3 TMD on the basis of combined Monte Carlo/atomistic MD simulations.[24]

It is important to consider possible methodological limitations. It is recognized that CG simulations provide an approximation to more detailed, all-atom treatments of helix–helix interfaces. However, recent studies suggest that the combined use of CG and subsequent atomistic simulations can accurately reproduce, e.g., the NMR structure of the integrin TMD heterodimer.[27] In part, this is because multiple CG simulations allow exploration of a greater range of conformational and helix-packing space than equivalent AT simulations would on their own. Furthermore, comparison of atomistic[18] and CG[19,20] simulations of glycophorin A dimerization suggests that the two methods yield comparable free energy profiles for the dimerization process. A further limitation is the use of a single simple phospholipid species in our simulations. Studies of, e.g., GPCRs have shown how lipid composition may influence receptor association and function,[53] and this is likely to also be important for the TMDs of receptor tyrosine kinases.[23] Thus, in future studies, it will be important to include consideration of the multiple lipid species present in cell membranes, and their likely interactions with both the transmembrane and juxtamembrane domains of FGFR3. However, it is likely that a full consideration of such lipid interactions and their influence on TMD dimerization will require more detailed characterization and comparison of energy landscapes of helix dimerization,[22] which in turn is likely to require the use of enhanced sampling protocols (see, e.g., ref 54), even when using CG simulations.

One aspect that may benefit from future investigations is that of the kinetics of TMD association and dissociation. Recent atomistic[14] simulations of EGFR TMDs show that >10 μs simulations are needed to observe TMD dimer dissociation events. Experimental observations of, e.g., dimerization of a model TMD peptide[55] or refolding of bacteriorhodopsin[56] suggest time scales in excess of 1 s. Clearly, a complete characterization of the mechanism of TMD association and dissociation by simulations will require enhanced sampling procedures, e.g., metadynamics.[57]

It is informative to compare our model of the FGFR3 TMD dimer with the structure revealed by NMR studies of the dimer in detergent (DPC/SDS) micelles.[8] In the NMR studies, a different interface, involving an extended hydrophobic heptad motif, is seen. However, in relating the NMR structure to pathogenic mutations, the authors of the NMR study[8] suggest the existence of an alternative packing mode involving a Gx_3G (or rather a small-x_3-small) sequence motif formed by residues G370-x_3-A374-x_3-S378-x_3-G382. This is the motif seen in our primary interface (Figure 4B) for the WT TMD. Thus, comparison of the NMR and the current simulation studies reinforces the suggestion that the FGFR3 TMDs may be able to adopt different packing modes, with changes in environment (e.g., bilayer vs micelle) or in interactions with the ectodomains (within the intact receptor) able to drive switching between

them. In particular, it seems likely that the primary packing mode mediated by a Gx_3G motif may correspond to an activated state of the receptor in terms of the effects of some pathogenic mutations located at this interface and by comparison with the proposed activated state structure of the EGFR TMD dimer, as discussed in more detail in ref 8.

The presence of multiple interaction modes of TMDs is an emergent theme for a number of RTKs and is likely to reflect the looser interactions between these helices than within the canonical tight binding interface of the GpA TMD dimer. This is likely to be functionally important, allowing a RTK TMD dimer to form a "multistate switch" that can be regulated by extracellular and intracellular interactions of the intact receptor. In particular, it seems that interactions of the intramembrane and juxtamembrane (JM) domains, with one another[14] and with lipids,[15] are likely to modulate the intrinsic TMD interactions. Our atomistic simulations indicate that the G380R mutation induces a movement of the receptor dimer toward the outer membrane leaflet, resulting in a rearrangement of the C-terminal CRLR residues. Whether this effect plays a role in the mechanism of pathogenesis of achondroplasia by triggering larger scale structural changes of the JM domains may be probed in future simulation studies.[58] Furthermore, the G380R mutation has been observed to cause a delay in FGFR3 downregulation,[59] possibly caused by altered interactions of the JM domain with intracellular components of this process.[60]

■ ASSOCIATED CONTENT

Supporting Information

Additional methodological details concerning analysis of the simulations and six figures presenting supplementary analysis of both the coarse-grained and atomistic simulations. This material is available free of charge via the Internet at http://pubs.acs.org.

■ AUTHOR INFORMATION

Corresponding Author

*E-mail: mark.sansom@bioch.ox.ac.uk. Phone: +44 1865 613306.

Present Address

[§]B.A.H.: Microsoft Research Cambridge, 21 Station Rd., Cambridge CB1 2FB, U.K.

Author Contributions

T.R. and S.M. performed the experiments and analyzed the data. A.B., B.A.H., and A.C. provided computational tools and protocols. T.R., S.M., and M.S.P.S. wrote the manuscript.

Funding

T.R. was supported by a Natural Sciences and Engineering Research Council of Canada (NSERC) Canada Graduate Scholarship D, a Killam Honorary Predoctoral Fellowship, and an NSERC Michael Smith Foreign Study Supplement and is currently supported by a Canadian Institutes of Health Research Postdoctoral Fellowship and a Fulford Junior Research Fellowship from Somerville College. S.M. is a Wellcome Trust graduate student, and M.S.P.S. acknowledges grants from the BBSRC and the Wellcome Trust. Additional computational resources were provided by ACEnet, the regional high-performance computing consortium for universities in Atlantic Canada. ACEnet is funded by the Canada Foundation for Innovation (CFI), the Atlantic Canada Opportunities Agency (ACOA), and the provinces of Newfoundland and Labrador, Nova Scotia, and New Brunswick.

Notes

The authors declare no competing financial interest.

■ ACKNOWLEDGMENTS

We thank Philip Fowler, Oliver Beckstein, Phillip Stansfeld, Antreas Kalli, Yvonne Jones, Khairul Adb Halim, and Dave Marshall for helpful discussions and suggestions and Jan K. Rainey for his critical reading of the manuscript.

■ REFERENCES

(1) Arkhipov, A., Shan, Y., Das, R., Endres, N. F., Eastwood, M. P., Wemmer, D. E., Kuriyan, J., and Shaw, D. E. (2013) Architecture and membrane interactions of the EGF receptor. *Cell 152*, 557−569.

(2) Mineev, K. S., Bocharov, E. V., and Arseniev, A. S. (2008) Spatial structure of the dimeric transmembrane domain of the growth factor receptor ErbB2 presumably corresponding to the receptor active state. *J. Biol. Chem. 283*, 6950−6956.

(3) Mineev, K. S., Bocharov, E. V., Pustovalova, Y. E., Bocharova, O. V., Chupin, V. V., and Arseniev, A. S. (2010) Spatial structure of the transmembrane domain heterodimer of ErbB1 and ErbB2 receptor tyrosine kinases. *J. Mol. Biol. 400*, 231−243.

(4) Mineev, K. S., Khabibullina, N. F., Lyukmanova, E. N., Dolgikh, D. A., Kirpichnikov, M. P., and Arseniev, A. S. (2011) Spatial structure and dimer-monomer equilibrium of the ErbB3 transmembrane domain in DPC micelles. *Biochim. Biophys. Acta 1808*, 2081−2088.

(5) Bocharov, E. V., Mineev, K. S., Goncharuk, M. V., and Arseniev, A. S. (2012) Structural and thermodynamic insight into the process of "weak" dimerization of the ErbB4 transmembrane domain by solution NMR. *Biochim. Biophys. Acta 1818*, 2158−2170.

(6) Bocharov, E. V., Mayzel, M. L., Volynsky, P. E., Goncharuk, M. V., Ermolyuk, Y. S., Schulga, A. A., Artemenko, E. O., Efremov, R. G., and Arseniev, A. S. (2008) Spatial structure and pH-dependent conformational diversity of dimeric transmembrane domain of the receptor tyrosine kinase EphA1. *J. Biol. Chem. 283*, 29385−29395.

(7) Bocharov, E. V., Mayzel, M. L., Volynsky, P. E., Mineev, K. S., Tkach, E. N., Ermolyuk, Y. S., Schulga, A. A., Efremov, R. G., and Arseniev, A. S. (2010) Left-handed dimer of EphA2 transmembrane domain: Helix packing diversity among receptor tyrosine kinases. *Biophys. J. 98*, 881−889.

(8) Bocharov, E. V., Lesovoy, D. M., Goncharuk, S. A., Goncharuk, M. V., Hristova, K., and Arseniev, A. S. (2013) Structure of FGFR3 transmembrane domain dimer: Implications for signaling and human pathologies. *Structure 21*, 2087−2093.

(9) Bellus, G. A., Hefferon, T. W., Deluna, R. I. O., Hecht, J. T., Horton, W. A., Machado, M., Kaitila, I., McIntosh, I., and Francomano, C. A. (1995) Achondroplasia is defined by recurrent G380R mutations of FGFR3. *Am. J. Hum. Genet. 56*, 368−373.

(10) Webster, M. K., and Donoghue, D. J. (1996) Constitutive activation of fibroblast growth factor receptor 3 by the transmembrane domain point mutation found in achondroplasia. *EMBO J. 15*, 520−527.

(11) You, M., Li, E., and Hristova, K. (2006) The achondroplasia mutation does not alter the dimerization energetics of the fibroblast growth factor receptor 3 transmembrane domain. *Biochemistry 45*, 5551−5556.

(12) Han, X., Mihailescu, M., and Hristova, K. (2006) Neutron diffraction studies of fluid bilayers with transmembrane proteins: Structural consequences of the achondroplasia mutation. *Biophys. J. 91*, 3736−3747.

(13) Sarabipour, S., and Hristova, K. (2013) FGFR3 transmembrane domain interactions persist in the presence of its extracellular domain. *Biophys. J. 105*, 165−171.

(14) Endres, N. F., Das, R., Smith, A. W., Arkhipov, A., Kovacs, E., Huang, Y. J., Pelton, J. G., Shan, Y. B., Shaw, D. E., Wemmer, D. E., Groves, J. T., and Kuriyan, J. (2013) Conformational coupling across

the plasma membrane in activation of the EGF receptor. *Cell 152*, 543−556.
(15) Matsushita, C., Tamagaki, H., Miyazawa, Y., Aimoto, S., Smith, S. O., and Sato, T. (2013) Transmembrane helix orientation influences membrane binding of the intracellular juxtamembrane domain in Neu receptor peptides. *Proc. Natl. Acad. Sci. U.S.A. 110*, 1646−1651.
(16) Zhang, L. Q., Sodt, A. J., Venable, R. M., Pastor, R. W., and Buck, M. (2013) Prediction, refinement, and persistency of transmembrane helix dimers in lipid bilayers using implicit and explicit solvent/lipid representations: Microsecond molecular dynamics simulations of ErbB1/B2 and EphA1. *Proteins: Struct., Funct., Bioinf. 81*, 365−376.
(17) Polyansky, A. A., Volynsky, P. E., and Efremov, R. G. (2012) Multistate organization of transmembrane helical protein dimers governed by the host membrane. *J. Am. Chem. Soc. 134*, 14390−14400.
(18) Hénin, J., Pohorille, A., and Chipot, C. (2005) Insights into the recognition and association of transmembrane α-helices. The free energy of α-helix dimerization in glycophorin A. *J. Am. Chem. Soc. 127*, 8478−8484.
(19) Janosi, L., Prakash, A., and Doxastakis, M. (2010) Lipid-modulated sequence-specific association of glycophorin A in membranes. *Biophys. J. 99*, 284−292.
(20) Sengupta, D., and Marrink, S. J. (2010) Lipid-mediated interactions tune the association of glycophorin A helix and its disruptive mutants in membranes. *Phys. Chem. Chem. Phys. 12*, 12987−12996.
(21) Psachoulia, E., Marshall, D., and Sansom, M. S. P. (2010) Molecular dynamics simulations of the dimerization of transmembrane α-helices. *Acc. Chem. Res. 43*, 388−396.
(22) Prakash, A., Janosi, L., and Doxastakis, M. (2010) Self-association of models of transmembrane domains of ErbB receptors in a lipid bilayer. *Biophys. J. 99*, 3657−3665.
(23) Prakash, A., Janosi, L., and Doxastakis, M. (2011) GxxxG motifs, phenylalanine, and cholesterol guide the self-association of transmembrane domains of ErbB2 receptors. *Biophys. J. 101*, 1949−1958.
(24) Volynsky, P. E., Polyansky, A. A., Fakhrutdinova, G. N., Bocharov, E., and Efremov, R. G. (2013) Role of dimerization efficiency of transmembrane domains in activation of fibroblast growth factor receptor 3. *J. Am. Chem. Soc. 135*, 8105−8108.
(25) Bond, P. J., Wee, C. L., and Sansom, M. S. P. (2008) Coarse-grained molecular dynamics simulations of the energetics of helix insertion into a lipid bilayer. *Biochemistry 47*, 11321−11331.
(26) Psachoulia, E., Bond, P. J., Fowler, P. W., and Sansom, M. S. P. (2008) Helix-helix interactions in membrane proteins: Coarse grained simulations of glycophorin helix dimerization. *Biochemistry 47*, 10503−105012.
(27) Kalli, A. C., Hall, B. A., Campbell, I. D., and Sansom, M. S. P. (2011) A helix heterodimer in a lipid bilayer: prediction of the structure of an integrin transmembrane domain via multiscale simulations. *Structure 19*, 1477−1484.
(28) Hess, B., Kutzner, C., van der Spoel, D., and Lindahl, E. (2008) GROMACS 4: Algorithms for highly efficient, load-balanced, and scalable molecular simulation. *J. Chem. Theory Comput. 4*, 435−447.
(29) Marrink, S. J., de Vries, A. H., and Mark, A. E. (2004) Coarse grained model for semiquantitative lipid simulations. *J. Phys. Chem. B 108*, 750−760.
(30) Marrink, S. J., Risselada, J., Yefimov, S., Tieleman, D. P., and de Vries, A. H. (2007) The MARTINI force field: Coarse grained model for biomolecular simulations. *J. Phys. Chem. B. 111*, 7812−7824.
(31) Monticelli, L., Kandasamy, S. K., Periole, X., Larson, R. G., Tieleman, D. P., and Marrink, S. J. (2008) The MARTINI coarse grained force field: Extension to proteins. *J. Chem. Theory Comput. 4*, 819−834.
(32) Berendsen, H. J. C., Postma, J. P. M., van Gunsteren, W. F., DiNola, A., and Haak, J. R. (1984) Molecular dynamics with coupling to an external bath. *J. Chem. Phys. 81*, 3684−3690.
(33) Reddy, T., and Rainey, J. K. (2012) Multifaceted substrate capture scheme of a rhomboid protease. *J. Phys. Chem. B 116*, 8942−8954.
(34) Stansfeld, P. J., and Sansom, M. S. P. (2011) From coarse-grained to atomistic: A serial multi-scale approach to membrane protein simulations. *J. Chem. Theory Comput. 7*, 1157−1166.
(35) Parrinello, M., and Rahman, A. (1981) Polymorphic transitions in single-crystals: A new molecular-dynamics method. *J. Appl. Phys. 52*, 7182−7190.
(36) Hess, B., Bekker, H., Berendsen, H. J. C., and Fraaije, J. G. E. M. (1997) LINCS: A linear constraint solver for molecular simulations. *J. Comput. Chem. 18*, 1463−1472.
(37) Scott, W. R. P., Hunenberger, P. H., Tironi, I. G., Mark, A. E., Billeter, S. R., Fennen, J., Torda, A. E., Huber, T., Kruger, P., and van Gunsteren, W. F. (1999) The GROMOS biomolecular simulation program package. *J. Phys. Chem. A 103*, 3596−3607.
(38) Michaud-Agrawal, N., Denning, E. J., Woolf, T. B., and Beckstein, O. (2011) MDAnalysis: A toolkit for the analysis of molecular dynamics simulations. *J. Comput. Chem. 32*, 2319−2327.
(39) Humphrey, W., Dalke, A., and Schulten, K. (1996) VMD: Visual Molecular Dynamics. *J. Mol. Graphics 14*, 33−38.
(40) MacKenzie, K. R., Prestegard, J. H., and Engelman, D. M. (1997) A transmembrane helix dimer: Structure and implications. *Science 276*, 131−133.
(41) Smith, S. O., Song, D., Shekar, S., Groesbeek, M., Ziliox, M., and Aimoto, S. (2001) Structure of the transmembrane dimer interface of glycophorin A in membrane bilayers. *Biochemistry 40*, 6553−6558.
(42) Finger, C., Escher, C., and Schneider, D. (2009) The single transmembrane domains of human tyrosine kinases encode self interactions. *Sci. Signaling 2* (ra56), 51−58.
(43) Treutlein, H. R., Lemmon, M. A., Engelman, D. M., and Brunger, A. T. (1992) The glycophorin A transmembrane domain dimer: Sequence specific propensity for a right handed supercoil of helices. *Biochemistry 31*, 12726−12733.
(44) Meyers, G. A., Orlow, S. J., Munro, I. R., Przylepa, K. A., and Jabs, E. W. (1995) Fibroblast-growth-factor-receptor-3 (FGFR3) transmembrane mutation in crouzon-syndrome with acanthosis nigricans. *Nat. Genet. 11*, 462−464.
(45) Martinez-Frias, M. L., de Frutos, C. A., Bermejo, E., and Nieto, M. A. (2010) Review of the recently defined molecular mechanisms underlying thanatophoric dysplasia and their potential therapeutic implications for achondroplasia. *Am. J. Med. Genet., Part A 152*, 245−255.
(46) Peng, W. C., Lin, X., and Torres, J. (2009) The strong dimerization of the transmembrane domain of the fibroblast growth factor receptor (FGFR) is modulated by C-terminal juxtamembrane residues. *Protein Sci. 18*, 450−459.
(47) You, M., Spangler, J., Li, E., Han, X., Ghosh, P., and Hristova, K. (2007) Effect of pathogenic cysteine mutations on FGFR3 transmembrane domain dimerization in detergents and lipid bilayers. *Biochemistry 46*, 11039−11046.
(48) Moriki, T., Maruyama, H., and Maruyama, I. N. (2001) Activation of preformed EGF receptor dimers by ligand-induced rotation of the transmembrane domain. *J. Mol. Biol. 311*, 1011−1026.
(49) Beevers, A. J., Damianoglou, A., Oates, J., Rodger, A., and Dixon, A. M. (2010) Sequence-dependent oligomerization of the Neu transmembrane domain suggests inhibition of "conformational switching" by an oncogenic mutant. *Biochemistry 49*, 2811−2820.
(50) Killian, J. A., and von Heijne, G. (2000) How proteins adapt to a membrane-water interface. *Trends Biochem. Sci. 25*, 429−434.
(51) Kim, C., Schmidt, T., Cho, E. G., Ye, F., Ulmer, T. S., and Ginsberg, M. H. (2012) Basic amino-acid side chains regulate transmembrane integrin signalling. *Nature 481*, 209−213.
(52) Ozdirekcan, S., Etchebest, C., Killian, J. A., and Fuchs, P. F. J. (2007) On the orientation of a designed transmembrane peptide: Toward the right tilt angle? *J. Am. Chem. Soc. 129*, 15174−15181.
(53) Botelho, A. V., Huber, T., Sakmar, T. P., and Brown, M. F. (2006) Curvature and hydrophobic forces drive oligomerization and modulate activity of rhodopsin in membranes. *Biophys. J. 91*, 4464−4477.
(54) Li, P. C., Miyashita, N., Im, W., Ishido, S., and Sugita, Y. (2013) Multidimensional umbrella sampling and replica-exchange molecular

dynamics simulations for structure prediction of transmembrane helix dimers. *J. Comput. Chem.*, 10.1002/jcc.23494.
(55) Tang, J., Yin, H., Qiu, J. D., Tucker, M. J., DeGrado, W. F., and Gai, F. (2009) Using two fluorescent probes to dissect the binding, insertion, and dimerization kinetics of a model membrane peptide. *J. Am. Chem. Soc. 131*, 3816−3817.
(56) Curnow, P., and Booth, P. J. (2007) Combined kinetic and thermodynamic analysis of α-helical membrane protein unfolding. *Proc. Natl. Acad. Sci. U.S.A. 104*, 18970−18975.
(57) Limongelli, V., Bonomi, M., and Parrinello, M. (2013) Funnel metadynamics as accurate binding free-energy method. *Proc. Natl. Acad. Sci. U.S.A. 110*, 6358−6363.
(58) Koldsö, H., and Sansom, M. S. P. (2012) Local lipid reorganization by a transmembrane protein domain. *J. Phys. Chem. Lett. 3*, 3498−3502.
(59) Monsonego-Ornan, E., Adar, R., Feferman, T., Segev, O., and Yayon, A. (2000) The transmembrane mutation G380R in fibroblast growth factor receptor 3 uncouples ligand-mediated receptor activation from down-regulation. *Mol. Cell. Biol. 20*, 516−522.
(60) Cho, J. Y., Guo, C. S., Torello, M., Lunstrum, G. P., Iwata, T., Deng, C. X., and Horton, W. A. (2004) Defective lysosomal targeting of activated fibroblast growth factor receptor 3 in achondroplasia. *Proc. Natl. Acad. Sci. U.S.A. 101*, 609−614.